# Oriented chiral water wires in artificial transmembrane channels

Istvan Kocsis, Mirco Sorci, Heather Vanselous, Samuel Murail, Stephanie Sanders, Erol Licsandru, Yves-Marie Legrand, Arie van Der Lee, Marc Baaden, Poul Petersen, et al.

▶ **To cite this version:**

Istvan Kocsis, Mirco Sorci, Heather Vanselous, Samuel Murail, Stephanie Sanders, et al.. Oriented chiral water wires in artificial transmembrane channels. Science Advances , 2018, 4 (3), pp.eaao5603. 10.1126/sciadv.aao5603 . hal-01797309

**HAL Id: hal-01797309**
**https://hal.umontpellier.fr/hal-01797309v1**

Submitted on 31 May 2021

**HAL** is a multi-disciplinary open access archive for the deposit and dissemination of scientific research documents, whether they are published or not. The documents may come from teaching and research institutions in France or abroad, or from public or private research centers.

L'archive ouverte pluridisciplinaire **HAL**, est destinée au dépôt et à la diffusion de documents scientifiques de niveau recherche, publiés ou non, émanant des établissements d'enseignement et de recherche français ou étrangers, des laboratoires publics ou privés.

Distributed under a Creative Commons Attribution - NonCommercial 4.0 International License

PHYSICS

# Oriented chiral water wires in artificial transmembrane channels

Istvan Kocsis,[1] Mirco Sorci,[2] Heather Vanselous,[3] Samuel Murail,[4] Stephanie E. Sanders,[3] Erol Licsandru,[1] Yves-Marie Legrand,[1] Arie van der Lee,[1] Marc Baaden,[4] Poul B. Petersen,[3]* Georges Belfort,[2]* Mihail Barboiu[1]*

Copyright © 2018 The Authors, some rights reserved; exclusive licensee American Association for the Advancement of Science. No claim to original U.S. Government Works. Distributed under a Creative Commons Attribution NonCommercial License 4.0 (CC BY-NC).

**Aquaporins (AQPs) feature highly selective water transport through cell membranes, where the dipolar orientation of structured water wires spanning the AQP pore is of considerable importance for the selective translocation of water over ions. We recently discovered that water permeability through artificial water channels formed by stacked imidazole I-quartet superstructures increases when the channel water molecules are highly organized. Correlating water structure with molecular transport is essential for understanding the underlying mechanisms of (fast) water translocation and channel selectivity. Chirality adds another factor enabling unique dipolar oriented water structures. We show that water molecules exhibit a dipolar oriented wire structure within chiral I-quartet water channels both in the solid state and embedded in supported lipid bilayer membranes (SLBs). X-ray single-crystal structures show that crystallographic water wires exhibit dipolar orientation, which is unique for chiral I-quartets. The integration of I-quartets into SLBs was monitored with a quartz crystal microbalance with dissipation, quantizing the amount of channel water molecules. Nonlinear sum-frequency generation vibrational spectroscopy demonstrates the first experimental observation of dipolar oriented water structures within artificial water channels inserted in bilayer membranes. Confirmation of the ordered confined water is obtained via molecular simulations, which provide quantitative measures of hydrogen bond strength, connectivity, and the stability of their dipolar alignment in a membrane environment. Together, uncovering the interplay between the dipolar aligned water structure and water transport through the self-assembled I-quartets is critical to understanding the behavior of natural membrane channels and will accelerate the systematic discovery for developing artificial water channels for water desalting.**

## INTRODUCTION

Water is of primordial importance in sustaining life (*1*). The molecular-scale interactions and hydrodynamics are crucial in mediating the structure of biomolecules and controlling important biological functions (*2*, *3*). Central to the properties of water are the structure and dynamics of the hydrogen-bonded network. The collective interactions of water with biomolecule interfaces render its structure and dynamics different from bulk water, as manifested in changes in the strength of the hydrogen-bonded network (*4*, *5*). Water in biological systems has specific functions in processes involving hydrophobicity, hydrogen bond self-assembly, and water transport (*6*, *7*).

An example is the selective transport of water with respect to ions from membrane potential gradients across biological pores such as aquaporins (AQPs) (*8*). In this context, it has previously been shown that natural AQPs can be mimicked using structurally simpler artificial compounds while displaying relatively high water flow rates and ionic exclusion (*9*–*11*). We previously reported that artificial imidazole quartets (I-quartets), that are stacks of four imidazoles and two water molecules, form a water channel in the lipid bilayer membranes (Fig. 1). These artificial I-quartets can stabilize oriented water wires within a 2.6 Å diameter pore (Fig. 1D) (*12*), which is very close to the narrowest constriction observed in AQPs (2.8 Å) (*13*). The channels can transport ~$10^6$ water molecules per second per channel, which is within two orders of magnitude of AQPs' transport rates, and reject all ions except protons (*14*). These self-assembled channels exhibit remarkable combinations of structural behavior such as dipolar orientation of confined water reminiscent of those observed in natural AQPs. They represent model systems of prime importance for enhancing water and proton translocation along oriented water wires (*14*). This dipolar orientation of water molecules within an artificial channel may furthermore adopt the supramolecular chirality of individual channels, whereas overall achiral structures with inverted symmetry contain opposing chiral oriented channels. Intrinsic chiral channels remove this restriction enabling the formation of unique chiral dipolar oriented water channels.

The present study targets the water dipolar orientation observed for the first time with x-ray crystallography of chiral single crystals of I-quartet artificial water channels and shows via chiral nonlinear vibrational spectroscopy that structured water wires are preserved when channels are embedded in bilayer membranes. Through a comprehensive experimental and computational study, we show that water wires under confinement, within chiral I-quartet artificial channels in the solid state or embedded in supported lipid bilayers (SLBs), form hydrogen-bonded chiral dipolar oriented water structures. The identification of chiral water structures within bilayer-embedded artificial water channels provides the inspiration for the supramolecular design of more effective self-assembled water channels. Controlling the water transport at the molecular level is extremely important for major technological applications, such as in efficient desalination systems.

## RESULTS

The present results provide a comprehensive description of the dipolar water orientation under confined conditions in artificial solid-state

[1]Institut Europeen des Membranes, Adaptive Supramolecular Nanosystems Group, Université de Montpellier, ENSCM, CNRS, Place Eugene Bataillon CC047, Montpellier F-34095, France. [2]Howard P. Isermann Department of Chemical and Biological Engineering and Center for Biotechnology and Interdisciplinary Studies, Rensselaer Polytechnic Institute, 110 Eighth Street, Troy, NY 12180–3590, USA. [3]Department of Chemistry and Chemical Biology, Cornell University, B46 Baker Laboratory, Ithaca, NY 14853, USA. [4]Laboratoire de Biochimie Théorique, CNRS, UPR9080, Université Paris Diderot, Sorbonne Paris Cité, Institut de Biologie Physico-Chimique, 13, rue Pierre et Marie Curie, Paris F-75005, France. *Corresponding author. Email: pbp33@cornell.edu (P.B.P.); belfog@rpi.edu (G.B.); mihail-dumitru.barboiu@umontpellier.fr (M.B.)

Downloaded from http://advances.sciencemag.org/ on May 31, 2021

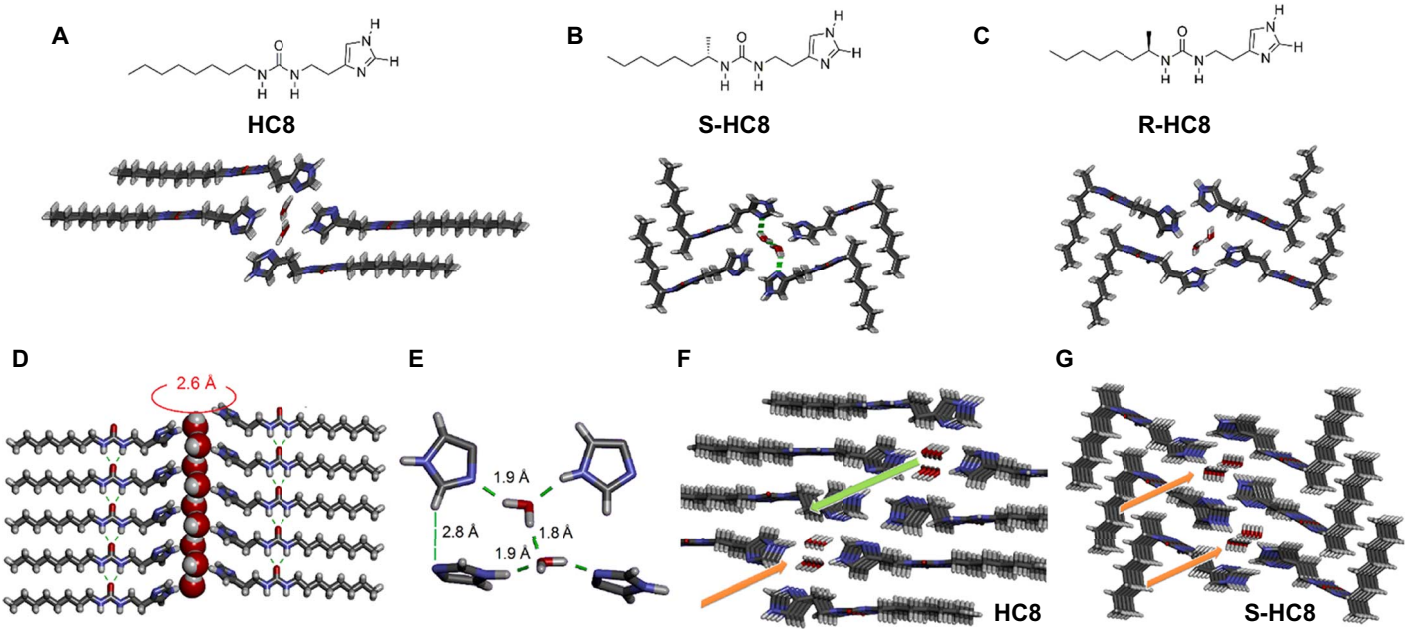


**Fig. 1. I-quartet artificial water channels and their chiral isomers packing.** Top views in stick representation (N, blue; C, gray; O, red; H, white) of the water-confined I-quartet x-ray single-crystal structures of (**A**) octylureido-ethylimidazole **HC8**, (**B**) S-octylureido-ethylimidazole **S-HC8**, and (**C**) R-octylureido-ethylimidazole **R-HC8** (*14*). (**D**) Side view in stick representation of planar arrays of the urea H-bonded ribbons of **HC8** showing that oriented water wires form along a 2.6 Å diameter pore of the channel. (**E**) Tetrameric H-bonded water I-quartet architectures confining dipolar oriented water. (**F**) Achiral centrosymmetric **HC8** I-quartets confining water wires of the opposite dipolar orientations, filling successive channels separated by water-free I-quartets and (**G**) chiral noncentrosymmetric **S-HC8** I-quartets confining oriented water wires with a unique dipolar orientation for total water-filled I-quartet channels.

I-quartet water channels that is maintained when the channels are embedded in the bilayer membranes. More specifically, x-ray single-crystal structures show the formation of self-assembled I-quartets confining dipolar water wires; quartz crystal microbalance with dissipation (QCM-D) experiments confirm the SLB formation and allow estimation of the amount of water present in the channels; and achiral and chiral sum-frequency generation (SFG) spectroscopy and complimenting molecular dynamics (MD) simulations provide quantitative measures of the hydrogen bond strength and interaction patterns, dipolar water orientation, and ordering, as well as on the electrostatic polarization imprinted on the dipolar water by their surroundings.

## X-ray single-crystal structures and water confinement in self-assembled I-quartets

I-quartet synthesis: Three compounds were prepared for this study (Fig. 1). The corresponding isocyanates were treated with histamine ($CH_3CN$/*N*,*N*-dimethylacetamide, 120°C, 5 hours) to afford crystallization of achiral **HC8** and chiral **R-HC8** or **S-HC8** compounds, as white powders. The NMR and electrospray ionization mass spectrometry spectra agree with the proposed formulas (*14*). Colorless single crystals of **HC8**, **R-HC8**, and **S-HC8** were obtained after recrystallization from water at room temperature.

The x-ray structure of **HC8** reveals that two conformers of **HC8** are present in the solid state: one elongated stretching to their maximum theoretical length, 19.8 Å, and one contracted at 19.1 Å presenting two gauche conformations (Fig. 1, A to C, and fig. S1). The crystal packing of chiral **R-HC8** (Fig. 1B) or **S-HC8** (Fig. 1C) reveals compact bent conformations with the heptyl chains orthogonally disposed to the urea moieties. The homomonomeric H-bonding association of the urea-urea planar ribbons of the neighboring ureas lie in the same plane with respect to one another, as previously observed (*15*). The NH—O=C–H-bond ($d_{O—H}$ of 1.90 Å) distances are the same along the ribbon and are consistent with other urea systems (*15*–*18*). Accordingly, continuous asymmetric layers of **HC8** and **R-HC8** or **S-HC8** are generated in the solid state, such that the imidazole moieties are positioned at one end of each ribbon and strong hydrophobic van der Waals interactions between the alkyl chains stabilize the ribbon-like superstructures on the opposite side.

Analysis of crystal structures of **HC8** and **R-HC8** or **S-HC8** further reveals unexpected –C-H—N motifs ($d_{N—HC}$ of 2.7 to 2.8 Å) between two orthogonally disposed imidazole moieties, resulting in the formation of imidazole dimers (Fig. 1D) reminiscent of the structures observed for the $His^{37}$-quartet proton gate of the Influenza A M2 protein (*19*, *20*). The oxygen atom of each water molecule is simultaneously strongly H-bonded to both imidazole NH groups ($d_{O—H}$ of 1.9 Å) and the vicinal water molecules ($d_{O—H}$ of 1.8 Å) (Fig. 1E). The symmetrical relative disposition of the imidazole dimers was previously observed for other compounds (*12*, *21*) and regulates the water molecules to be statistically restricted to two orientations of opposite chiralities in such a way that the water wires within the same channel present a unique dipolar orientation. Here, on the other hand, the relative asymmetric structures of the imidazole dimers in the self-assembled **HC8** and **R-HC8** or **S-HC8** compounds determine a unique dipolar orientation of the water molecules comprising a crystallographic 100% occupancy of both water H atoms bonded to N-imidazoles and neighboring water molecules (Fig. 1E). Each individual I-quartet channel is supramolecularly chiral and contains dipolar water wires oriented in one direction. The overall structure of achiral compound **HC8** is centrosymmetric, so that the water wires of the opposite water dipolar orientations are present in successive enantiomeric water-filled

Downloaded from http://advances.sciencemag.org/ on May 31, 2021

channels, separated by water-free I-quartets (Fig. 1F). In contrast, the noncentrosymmetric structures of chiral compounds **R-HC8** and **S-HC8** show a unique dipolar orientation for all water-filled I-quartet channels (Fig. 1G).

Note that water molecules form a more compact water wire motif in **R-HC8** and **S-HC8** compared with **HC8**. The I-quartet water channels of rhomboidal shape (20.1 × 22.9 Å$^2$ for **HC8** and 22.4 × 14.9 Å$^2$ for **R-HC8** and **S-HC8**, considering a projection in a plane and not taking into account the van der Waals radii of terminal sites) determine a pore gap in the 2.6 Å channel, very close to the narrowest constriction observed in AQP water channels (2.8 Å) perfectly accommodating water wires' binding and conduction (*22*, *23*). Moreover, these structures confirm that precise interactions constrain the orientation of water molecules that move collectively while maintaining H-bond interactions within the I-quartet pore. A similar occupancy by partially hydrated cations would imply a change in the energy difference between H-bonding configurations of hydrated cations in the I-quartet pore. The binding behavior of I-quartets is optimal for maximizing the pure water translocation rates (*24*). From the x-ray single-crystal data of the I-quartets reported here, it can be concluded that (i) the water structure in individual channels of both chiral **R-HC8** and **S-HC8** or achiral **HC8** imidazoles form oriented water wires. Such a directional chiral ordering of confined water is imposed by relative positioning of the imidazole dimers within the channel. (ii) For **HC8**, because of the symmetry inversion centers, two vicinal water–filled channels are oppositely oriented, so a racemic mixture of water wires of both chiralities are present, whereas for the chiral nonsymmetric **R-HC8** and **S-HC8** channels, water wires present a unique dipolar orientation of all successive channels (Fig. 1, F and G).

## I-quartet incorporation into SLBs

We know that the I-quartet channels are spontaneously inserted into lipid bilayers (*12*, *14*). Among the various methods that can be used to analyze the interactions between the I-quartets and an SLB, the QCM-D technique (*25*–*27*) allows detection of mass changes at the sensor surface based on the reciprocal piezoelectric effect (*28*). As previously observed, the formation of the SLB from small unilamellar vesicles (SUVs) follows a two-step mechanism: (i) fast adsorption of the SUVs to the QCM-D silica crystal with increased mass (that is, decreased Δ*F*, frequency) and increased layer flexibility (that is, increased Δ*D*, dissipation coefficient), because floppy SUVs were deposited on the QCM-D sensor, and (ii) rupture and fusion of SUVs into SLBs (Δ*F* minimum and Δ*D* maximum) (Fig. 2) (*25*). A final buffer wash was included to allow complete annealing of the SLB (*29*, *30*). In particular, for the case of a molar composition of 4:1 = phosphatidylcholine (PC)/phosphatidylserine (PS) and **HC8**, a Δ*F* of −25.3 Hz was observed (Fig. 2B), corresponding to a total mass of 352 ng (that is, $m_L$ = 217 ng, $m_{HC8}$ = 54 ng, $m_{W,hydration\ layer}$ = 79 ng, and $m_{W,channel}$ = 1.8 ng), which demonstrated the formation of a stable SLB on the QCM-D surface (the calculations were based on the total insertion of **HC8** into the vesicles). The formation of an SLB, with or without **HC8**, was also tested for 4:1 = PC/PS + 20% w/w cholesterol (Chl) and PC (fig. S2). Whereas the addition of Chl did not affect the formation of an SLB, the PC-alone SUVs failed to form an SLB. In addition, on the basis of the Δ*F* values, the addition of **HC8** caused a decrease of the bilayer thickness from 4.61 nm (that is, 4:1 = PC/PS alone) to 4.48 nm (4:1 = PC/PS with **HC8**) (see paragraph 2.4.1 in note S1 of the Supplementary Materials). This measure demonstrated the formation of a more compact structure and the partial contraction of the SLB when **HC8** was incorporated. A more compact structure compared with the pure SLB is most likely the result

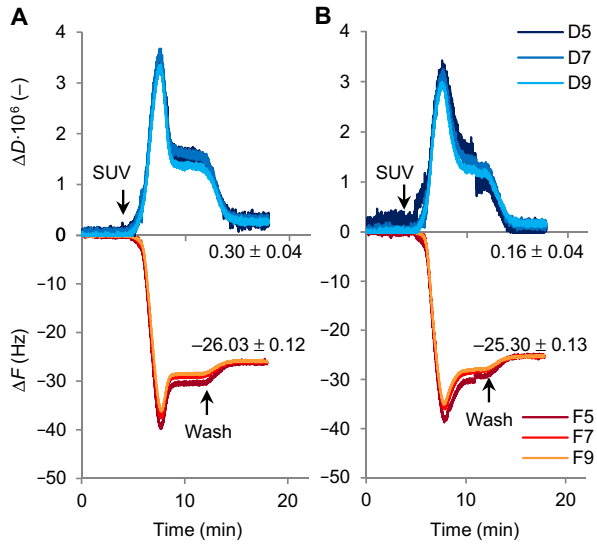


**Fig. 2. Incorporation of HC8 I-quartets in 4:1 = PC/PS SLB.** Experimental QCM-D frequency, Δ*F* (hertz) and dissipation coefficient, Δ*D* (–) shifts associated with the SLB formation on silica QCM-D sensors via fusion of SUVs of mixtures of lipids: (**A**) PC/PS, 4:1 mol/mol, and (**B**) PC/PS, 4:1 mol/mol + HC8. The two arrows for each panel indicate (i) SUV injection at 4 min and (ii) the washing step with 10 mM phosphate buffer (pH 6.4) after 12 min. Data of the fifth, seventh, and ninth overtones are shown for Δ*F* (F5, F7, and F9) and Δ*D* (D5, D7, and D9). SUV concentration was 0.2 mg/ml. Flow rate was kept constant at 100 μl/min.

of global SLB stabilization via supplementary phospholipid headgroup/imidazole electrostatic interactions and hydrophobic contact between the lipid and alkyl tails toward the bilayer aggregation. Together, these results demonstrate the incorporation of I-quartet channels into a supported 4:1 = PC/PS SLB that was selected for SFG experiments presented below. About 0.7% of the total mass of the SLBs comprises water wires in the system (see note S1 and figs. S2 to S5 for detailed calculations).

## Water structure and behavior in confined I-quartets

The hydrogen-bonded structure of water inside the channels is accurately characterized by the vibrational frequencies of the OH stretching vibrations, which are very sensitive to the local hydrogen-bonded network. Here, a strong correlation exists between the OH stretch frequency and the strength of the hydrogen bond. Non–hydrogen-bonded OH vibrations exhibit frequencies around 3700 cm$^{-1}$, which, upon hydrogen bonding, can shift down to 3000 cm$^{-1}$ depending on the strength of the hydrogen bond (*31*). Furthermore, specific hydrogen-bonded configurations exhibit distinct but broad and overlapping OH vibrational bands. Accordingly, the spectrum of OH stretch vibrations captures the overall water structure and distribution of hydrogen bond environments within the system, in this case water within artificial membrane channels and at the membrane surface.

Vibrational SFG spectroscopy involves nonlinear mixing of an infrared and a visible electric field, giving rise to the emission of photons at the sum of the two input frequencies (*32*, *33*). Within the dipole approximation, SFG requires broken inversion symmetry. Accordingly, SFG is surface-specific for liquids, because the interface necessarily breaks the average inversion symmetry found in the bulk liquid. This means that SFG spectroscopy is intrinsically sensitive to molecular dipole ordering, with the signal strength increasing with an increase in order. SFG spectroscopy is also a sensitive probe of chirality, because chirality breaks

Downloaded from http://advances.sciencemag.org/ on May 31, 2021

inversion symmetry (*34*, *35*). By controlling the polarization of three involved fields, we can selectively study achiral and chiral molecular structures. Polarization combinations are given in decreasing order of frequency, that is, the polarization of SFG, visible, and infrared fields, respectively. Here, polarization combinations that involve an odd number of p-polarized fields (*ssp*, *sps*, *pss*, and *ppp*) probe achiral molecular orientations, and polarization combinations that involve two p-polarized fields (*pps*, *psp*, and *spp*) only give rise to a signal if the molecular structure is chiral (*sss* is intrinsically zero for surfaces with $C_{\infty}$ symmetry).

To understand the structure of the water wires under confinement, we collected the SFG spectra of the achiral **HC8** and chiral **S-HC8** I-quartets inserted in SLB together, as well as of the reference SLB without channels. We measured four different pure polarization combinations: the achiral combinations *ppp* and *ssp* (Fig. 3, A and B) and the chiral combinations *psp* and *spp* (Fig. 3, C and D). Measuring two different polarization combinations for the achiral and chiral combinations provides information on the alignment of the vibrations (perpendicular to or with a shallow angle with respect to the surface) depending on the symmetry of the functional group. We also measured mixed polarization combinations interfering achiral and chiral responses to further validate the observed chiral structures, as discussed in the Supplementary Materials.

We examined the spectral region (2550 to 4000 $cm^{-1}$) covering the strong OH and NH stretches, with very weak CH stretches observed in the 2800- to 3000-$cm^{-1}$ range. For the lipid bilayer without channels, we observe in Fig. 3 the typical 3200-$cm^{-1}$ (yellow) and 3450-$cm^{-1}$ (green) bands observed for aqueous interfaces in both achiral *ppp* and *ssp* polarization combinations. Some controversy exists over the nature of the two features found at the air-water interface, where they merge into one for isotopic dilute HOD in $D_2O$. This suggests that the distinct features are caused by inter- and intramolecular couplings between the OH vibrations (*36*) or alternatively due to a Fermi-resonance with the OH bend (*37*). For the water-bilayer interface, the two features could be due to the same couplings or Fermi resonance but are likely due to specific subpopulations of bulk-like water molecules oriented in the field of the charged head groups and water molecules directly interacting with the lipid head groups, respectively. Irrespective of the nature of the two distinct features, the overall distribution of vibrational frequencies reflects the breadth of hydrogen bonding interactions at the water-bilayer interface. In addition to these two bands, we observe in Fig. 3 a band at 3650 $cm^{-1}$ (blue) that has previously been attributed to weakly hydrogen-bonded water molecules interacting with the ester carbonyl groups of the lipid.

For both samples with the artificial channels inserted into the SLB, we observe a large increase in the SFG intensity across the whole spectral region. In particular, the 3450-$cm^{-1}$ band increases, which is consistent with chain-like water wires inside the channel. In addition to three bands observed for the bilayer, we observed an additional sharp feature at 3750 $cm^{-1}$ (violet) in both *ppp* and *ssp*. This sharp feature is due to non–hydrogen-bonded OH groups, attributed to a subpopulation of the water molecules inside the channel lacking a donor hydrogen bond (Figs. 1D, 3E, and 4A). Furthermore, we observe a broad feature at 2800 $cm^{-1}$ in *ssp* but not in *ppp*. This feature is due to the imidazole groups of the channel itself and is also seen in the Fourier transform infrared (FTIR) spectrum of the dry imidazole powder; see the Supplementary Materials (fig. S8B). The observation of this feature in *ssp* but not *ppp* validates the I-quartet channels' orientation perpendicular to the lipid bilayer. Overall, the very large increase in the SFG intensity across the OH spectral region confirms that the insertion of the channels does not disrupt the order of the bilayer but rather proves that the hydrogen-bonded structure of the water molecules inside the channels is highly oriented with a strong dipolar alignment. Furthermore, the large SFG response shows that the dipolar ordering of the water wires inside the channels are aligned in the same direction. If alternate channels have opposite orientations, as one would expect for a free-standing bilayer, then the achiral SFG signal would vanish because of cancelation within the coherence length (70 nm) of the SFG experiments. This analysis is corroborated by the similar achiral SFG strengths of the **HC8** and **S-HC8** channels, which show that the dipolar alignment of the water wires in the supported bilayers is similar, whereas it is known not to be the case for free-standing bilayers.

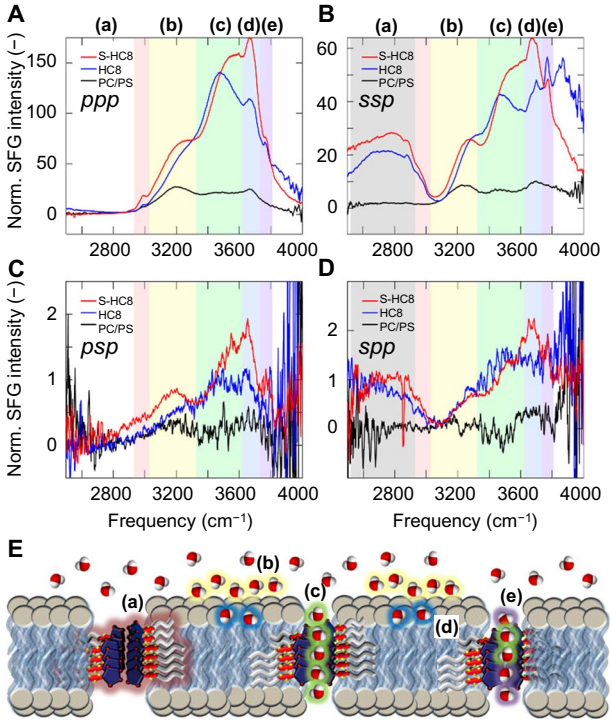


**Fig. 3. SFG vibrational spectroscopy.** SFG spectra of 4:1 = PC/PS SLB (reference), HC8, and S-HC8 I-quartets in 4:1 = PC/PS SLB determined for pure achiral (**A**) *ppp* and (**B**) *ssp*, as well as pure chiral (**C**) *psp* and (**D**) *spp* polarization combinations. (**E**) Highlighted regions describe (a) imidazole groups of the channel perpendicular to the lipid bilayer, (b) water orientated by the headgroup charges, (c) hydrogen bond chain-like channel water molecules, (d) weakly hydrogen-bonded water molecules interacting with the ester carbonyl groups of the lipids or less likely the imidazole carbonyls, and (e) non–hydrogen-bonded OH groups of water in the channel environment.

In the *psp* chiral SFG polarization combination (Fig. 3C), we observe a weak but nonzero chiral signal for the lipid bilayer without channels. This signal is caused by the chiral headgroups of the lipids inducing a chiral-polarized arrangement of water molecules near the polar region of the bilayer. The presence of the 2800-$cm^{-1}$ stretching band in the chiral *spp* polarized spectra of the **HC8** and **S-HC8** channels (Fig. 3D) shows that both channels exhibit a net chiral ordering in the SLB. Although this feature is expected for the **S-HC8** channel, this ordering shows that in addition to inducing a dipolar alignment of the water wires, the supported bilayer breaks the symmetry and also induces a net chirality for the **HC8** channel (Fig. 3E).

The chiral SFG responses of the OH features in the bilayers with the **HC8** and **S-HC8** channels in both *psp* and *spp* are much stronger

Downloaded from http://advances.sciencemag.org/ on May 31, 2021

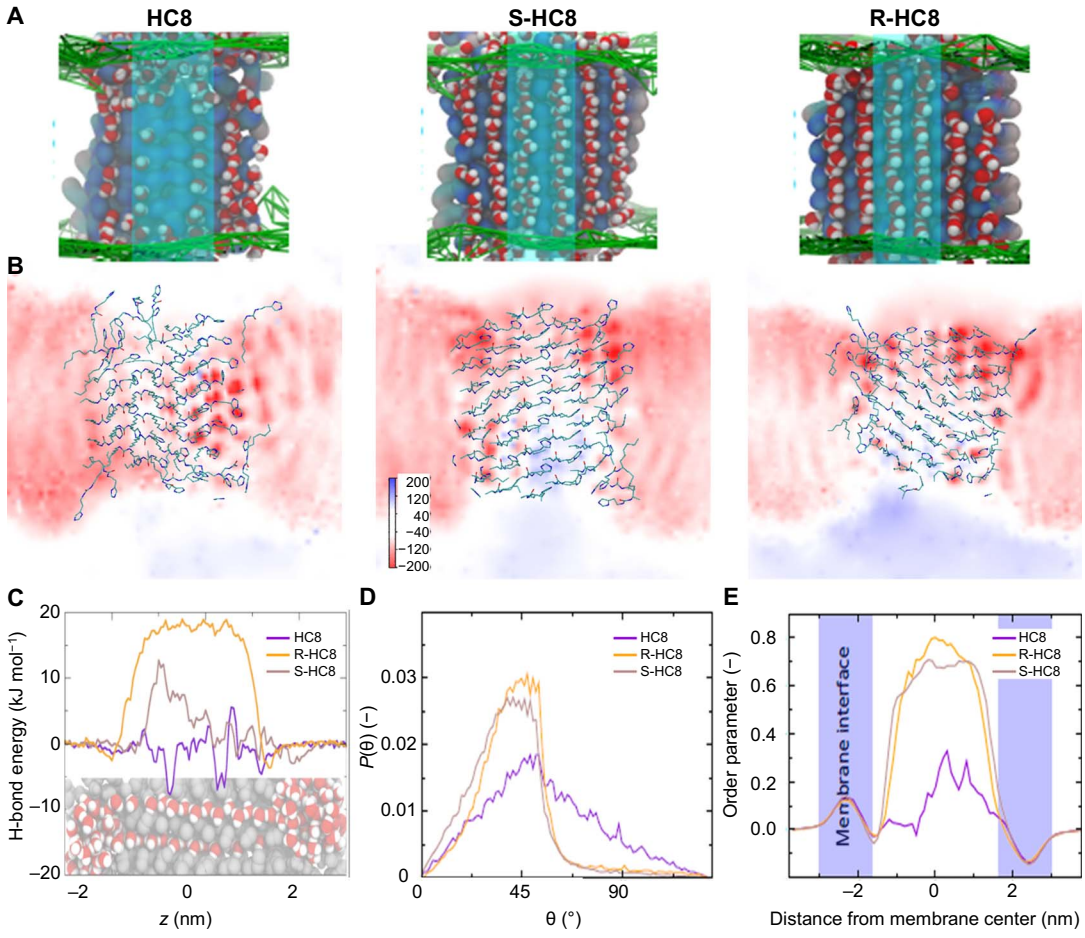


**Fig. 4. Molecular dynamics.** MD simulations of the I-quartets feature well-structured central water wires through these artificial channels depicted in (**A**). The region considered for analysis is highlighted by a cyan transparent rectangle. (**B**) Electrostatic potential field across the membrane and water channel region for **HC8**, **S-HC8**, and **R-HC8** systems. (**C**) Hydrogen bond energy depicting the stabilization of the two central water channels as compared to bulk water averaged over the 450- to 500-ns time frames. The *x* axis is the direction perpendicular to the membrane plane. Hydrogen bonds were calculated for the colored water molecules with their surroundings (gray atoms). (**D**) Distribution of O-H orientation angles (as defined in fig. S9A) for the water molecules within the transmembrane region of **HC8**, **S-HC8**, and **R-HC8** systems. Only the smallest of both orientation angles is reported. (**E**) Order parameters for water molecules within the membrane region calculated in the direction normal to the membrane plane.

compared with the bilayer without channels. This observation proves that the water dipoles are not only aligned inside the channels but also that they form a chiral water superstructure templated by the I-quartet channel. Although the chiral *psp* response is stronger for **S-HC8**, as expected, the *psp* response of **HC8** is significant and in *spp* the chiral SFG responses for both channels are similar. This finding is perhaps initially surprising. However, we know that each individual **HC8** channel is chiral in the solid crystal structures and successive enantiomeric channels of opposite chirality are separated by water-free I-quartets. When **HC8** is embedded in the bilayer membrane, the chiral polar region of lipids at the surface induces the amplification for one orientation that would preferentially form one chirality over another. In contrast, the noncentrosymmetric structures of chiral **S-HC8** show a unique dipolar orientation for all water-filled channels, and correspondingly, the chiral response of the **S-HC8** channels is larger compared with the achiral **HC8** channel.

## MD simulations

We measured several characteristics of water molecules and imidazoles in the MD simulations (table S4). The number of water molecules within the membrane region is similar for the **R-HC8** and **S-HC8** constructs, 68 and 65, respectively, and is significantly higher than for the **HC8** system featuring 39 water molecules. This results in the formation of water wires of roughly 3.5 nm in length, much longer than the length of ~1.0 nm of the water wires observed in the selectivity filter of AQP (*22*). We previously characterized the structure of I-quartet channels in the membrane region and concluded that the most representative channels in our simulation setup are the two central ones, which are less perturbed by boundary effects than the more exposed lateral ones (*14*). Hence, most of the simulation analysis focuses on these two central channels depicted in Fig. 4A. The visually apparent water ordering and orientation is in part due to anchoring sites provided by the imidazole structure across the membrane. Another contribution to water structuring originates in the electrostatic field generated by the ensemble of charges in the I-quartet system as depicted in Fig. 4B. A positive to negative potential field gradient builds up from bottom to top, driven by an additive effect of the orientation and ordering of imidazole dipoles, which seems to be highly correlated with the membrane contractions observed from QCM-D experiments. Qualitatively, this effect seems

Downloaded from http://advances.sciencemag.org/ on May 31, 2021

proportional to the preserved ordering of the imidazoles and decreases from **R-HC8** to **S-HC8** and **HC8**.

The hydrogen bonding patterns were analyzed in terms of water-water hydrogen bonds, water (donor)–to–imidazole (acceptor) hydrogen bonds, imidazole (donor)–to–water (acceptor) hydrogen bonds, and water-lipid interactions (table S5 and fig. S8B). As can be seen, the **R-HC8** and **S-HC8** constructs have comparable patterns with 1.4 and 1.6 hydrogen bonds on average connecting the pore waters and 1.9/1.8 hydrogen bonds linking them to the imidazoles. With 0.9 water-water hydrogen bonds on average, the water cohesion is significantly lower for the **HC8** system. The anchoring to the imidazoles is also of lower magnitude. Hydrogen bonds with lipids are not observed for these channels. Looking at the overall number of hydrogen bonds for the water molecules—compared to a reference value of 3.2 for bulk solvent, we notice that water in the **R-HC8** pore is unperturbed and, for the **S-HC8** pore, even stabilized, reaching up to 3.2 and 3.4 hydrogen bonds, respectively, whereas the **HC8** system lacks almost an entire hydrogen bond, correlating to the nonbonded water molecules observed with SFG spectroscopy.

Table S4 further provides data on the interactions formed by imidazoles, either among themselves, with lipids, or with water molecules. The overall number of hydrogen bonds is the same for all three systems, yet the imidazole-imidazole cohesion is higher for **R-HC8** and **S-HC8** compared with **HC8**. As a consequence, interaction with water is slightly less in the former two systems. Table S5 provides interaction statistics for the central versus lateral channels. The difference between the **HC8** and **R-/S-HC8** channels is marked more strongly than in the global analysis of table S4. Water-water cohesion is higher in the latter two, as well as in interactions with imidazoles. The central channels feature a strong overall involvement of water molecules in hydrogen bonds, as strong as or even beyond the pattern observed in bulk water.

We analyzed the strength of the hydrogen bonds for each water molecule in a cylindrical selection around the two central channels. Figure 4C depicts the hydrogen bond energy difference compared with the bulk water hydrogen bond energy taken as reference projected along the membrane normal direction (positive energy values represent stronger hydrogen bonds in this figure). The **S-HC8** system exhibits a strong and constant stabilization of the water molecules of almost 20 kJ/mol for the two central channels. For **R-HC8**, the stabilization varies from a maximum of about 13 kJ/mol down to 0 kJ/mol as in bulk water, which is due to an increased mobility—and hence destabilization—of the channel water molecules on one side of the membrane. For **HC8**, the hydrogen bond energy is fluctuating with a global tendency to be slightly less stable than in bulk water. Compared to bulk water, the hydrogen bond stabilization energies averaged over the central pore–inserted waters from about $z = -1.2$ to 0.8 nm are +17.6, +4.6, and −1.3 kJ/mol for **S-HC8**, **R-HC8**, and **HC8**, respectively.

We then characterized the orientation of the water molecules in the membrane region through the angle their O–H bonds form with the vector perpendicular to the membrane plane as illustrated in fig. S9A. On the basis of the smallest of both angles measured according to this scheme, we plotted the distributions for the **HC8**, **R-HC8**, and **S-HC8** systems calculated for the 450- to 500-ns time frame (Fig. 4D and fig. S9B). The apparent order, assessed by the width of the angle distribution, decreases slightly from **S-HC8** to **R-HC8** and then significantly to **HC8**. Furthermore, the distributions for the chiral systems are much narrower when centered around ~45°, falling off quickly for larger angles. The **HC8** distribution is much broader spreading up to 135°, indicating an almost random orientation for this system. We carried out further analysis of water molecule ordering through calculation of the order parameter of the water molecules. Figure 4E and fig. S9C show a marked ordering for **R-/S-HC8** systems, with a slightly higher ordering of **S-HC8**, compared with a rather flat profile for **HC8**. A specific pattern of water ordering is observed for the headgroup regions.

Together, these elements indicate a very strong patterning in the **S-HC8** system, reaching almost a perfectly stabilized and strongly oriented water wire. The chiral compatibility of the **S-HC8** system with the L-type lipids probably better stabilizes the respective I-quartet channel that adopts a conformation, where water molecules are more strongly associated than in bulk water. The **R-HC8** system maintains a strong dipolar orientation with fine-tuned interactions along the water wire, comparable energetics with respect to bulk water, and hence an increased mobility along a structured water path. The **HC8** channels are slightly destabilized compared with bulk water and do not form stable wire arrangements in the unsupported lipid bilayers.

## DISCUSSION

The present study provides the first observation of chiral dipole orientated water wires within artificial water channels under ambient bilayer membrane conditions. The dipolar water alignment within the membrane is driven by the orientation and ordering of imidazole/water dipoles. These results demonstrate that the water dipolar orientation is preserved from the single-crystal structures to the inherently dynamical water wires confined in artificial water channels in bilayer membranes. Overall, this system parallels the world of water transport through natural proteins, where the picture of dipolar water structures confined within a pore is the basis of the high permeability/selectivity of AQPs (*24*). Our results underline the chirality translation from lipids to I-quartet channels and from channels to structured dipolar water wires. First, we observe from the x-ray single-crystal structures that induced chirality in the channels and the structured water in the channel pores adapt accordingly. Here, the chiral backbone of the chiral **S-HC8** channels induces a unique chiral dipolar orientation for water wires along the axis of the pores as compared with the achiral **HC8** channels that present alternating chiral dipole orientations of water wires. This architecture further translated into a performance difference when assessing water permeability: the net permeabilities of **HC8** and its chiral isomers **R-HC8** and **S-HC8** at a channel-to-lipid weight ratio of 1 were 1.0 ± 0.3 μm/s, 2.8 ± 0.7 μm/s, and 4.1 ± 0.2 μm/s, as previously determined (*14*). The MD simulations have further shown that these subtle differences in structure can induce energetic differences when considering the strength of the hydrogen bonding network in the confinement region of the channels. The well-structured water wires in the **S-HC8** channels have an almost unperturbed behavior, with water flowing freely without significant energy penalties. This observation is mainly due to the fact that water found in the pores has 3.2 to 3.4 hydrogen bonds, which are very similar to the hydrogen bonds that occur in bulk water. On the other hand, **HC8** offers a rather less favorable confinement and stabilization for the water wires. The strong water dipole alignment inside the channels is confirmed by the SFG results, where the signal intensity is higher for both chiral and achiral dipolar water wires, as well as strongly bound water molecules in the case of the **S-HC8** embedded SLBs compared with the reference SLB. The SLBs are supported on a $CaF_2$ prism coated with a 100-nm layer of $SiO_2$, produce an asymmetry in the entire system, and induce a weak chiral alignment in the interfacial water structure through the chiral constituent lipids. The confined water wires in both the **HC8** and the **S-HC8** channels furthermore exhibit a strong chiral ordering template by the chiral channel structure.

Downloaded from http://advances.sciencemag.org/ on May 31, 2021

A significant difference in chiral ordering for the dipolar water wires in the **HC8** and **S-HC8** channels was expected because of the enantiomeric distribution of the water wires in the achiral **HC8** channel canceling the chiral signal as opposed to the water wires in the **S-HC8** channels containing a single chirality. Thus, chiral ordering was stronger in the **S-HC8** channels than in the **HC8** channels; however, a significant chiral ordering in the **HC8** channels was also observed. We hypothesize that the chirality of the lipids and the asymmetry of the solid support imposed a bias on the racemic mixture of **HC8** channels favoring one chirality over the other, thus activating them in SFG. These findings indicate that dipolar orientation of water is a general phenomenon related to chiral I quartet channels in which continual water wires are formed similar to AQP pores (*22*, *23*).

## CONCLUSIONS

A barrier to develop bioinspired synthetic systems lies in deciphering the complexity of natural systems. The findings presented here increase our understanding toward biomimicking the water structure within the extremely efficient AQPs, which remains an important exploratory challenge. The I-quartet artificial water channel provides remarkable combinations of functions very close to those encountered in natural AQPs and provides a simplified system, where the structural alignment of confined water can be elucidated and quantified. Our comprehensive study shows that self-assembled I-quartets embedded into lipid bilayers form highly ordered structures containing chiral dipolar oriented water wires. Our complementary x-ray single-crystal, QCM-D, MD, and nonlinear SFG spectroscopic studies presented here provide the first insight into the hydrogen-bonded structure and dipolar orientation of the water molecules inside the I-quartet channels in the lipid membrane environment at a molecular level.

On a more general note, chirality is a fundamental feature of biomolecules. The net dipolar ordering of confined water inside chiral I-quartet water channels can be generalized to water templated on biological surfaces/pockets, as recently demonstrated for DNA (*38*). The net dipolar orientation induced specific polarization of the channel, that likely acts as a driving force for water permeation through dielectrically asymmetric bilayer membranes. We show that the chiral structure of the I-quartets is transferred to the water, forming overall chiral dipolar water wires. Furthermore, we observe that the chirality of the headgroups of an SLB imparts a chiral selection onto a racemic mixture of enantiomeric water channels.

Through the correlation of energetically favorable confinement with induced dipole orientation of water molecules, I-quartet artificial water channels could be an interesting scaffold for future highly efficient water purification membranes. To compete with reverse osmosis, the current gold standard for desalinating seawater (*39*), permeation water flux rates for artificial water wire channels will need to be increased significantly to that of AQPs. Shorter channel lengths, more dense channels per unit area of surface, and optimal number of hydrogen bonds between the water and the channel [to take advantage of both selectivity in hydrophilic channels like I-quartets (*14*) and high water transport rates in hydrophobic channels such as carbon nanotubes (*40*)] are possible approaches.

## MATERIALS AND METHODS

Histamine, octyl, and R- and S-octan-2-yl isocyanates were purchased from Sigma-Aldrich Co. PC (chicken egg), PS (porcine brain), and Chl were purchased from Avanti Polar Lipids. Trizma hydrochloride, Trizma base, sodium phosphate monobasic, sodium phosphate dibasic, NaCl, Hepes, calcein, EDTA, Triton X-100, SDS, $D_2O$, ethanol, and chloroform were purchased from Sigma-Aldrich Co. Compressed $N_2$, He, and $O_2$ were supplied by Airgas. All buffers were prepared fresh and filtered through a 0.22-μm polyethersulfone membrane (Express PLUS, Millipore). For the SFG experiments, PBS (phosphate-buffered saline) and SDS were purchased from Sigma-Aldrich Co. Sodium chloride was purchased from Mallinckrodt Chemicals. Ultrapure water (Millipore MilliQ, 18.2 megohms·cm, ≤ 5 parts per billion total organic carbon) was used for all solutions. Equilateral $CaF_2$ prisms were obtained from Crystran Ltd.

### X-ray diffraction data

Data for the structures were collected on a Rigaku Oxford Diffraction Gemini-S S1 diffractometer with a Sapphire3 detector. Cu-Kα radiation was used with a graphite monochromator and a fiber-optics Mo-Enhance collimator for HC8. The data for S-HC8 and R-HC8 were collected with synchrotron radiation (λ = 0. 78965 Å) at the CRYSTAL beamline of Soleil. Data were corrected for absorption with CrysAlisPRO (*41*), and the structures were solved by iterative charge-flipping methods with Superflip (*42*). The structure refinements were carried out with CRYSTALS (*43*), and all nonhydrogen atoms were refined by full-matrix least squares on *F* using reflections with $I > 2\sigma(I)$ (table S1).

The crystals of **HC8** were tiny and scattered only weakly as diffracting crystals. Despite ~60 hours of prolonged measurement, no observable data were observed beyond 1.05 Å. Having acceptable data up to 0.83 Å would have required a measurement of several weeks, and therefore, a data strategy up to 1.0 Å only was used. The crystal structure displayed acceptable atomic displacement ellipsoids, so the relatively low data resolution does not appear to have an influence on the structure quality. For the structure of **S-HC8**, the terminal imidazole ring of both independent molecules appeared to be disordered over two independent positions, which also implied that two different sets of water molecules were present in the channels. The relative occupancies of the positionally disordered phenyl rings were approximately 0.8/0.2 in both cases. A number of distance and vibration restraints were used to keep an acceptable geometry of the rings and reasonable atomic displacement parameters. Because the anomalous scattering was negligible for the used x-ray wavelength, the absolute configuration was set in such a way as to be in agreement with the MD simulations reported by Licsandru *et al.* (*14*), notably concerning the orientation of the water molecules in the channel. The crystals of **R-HC8** were also tiny and weakly scattering even with synchrotron data, producing only a very low mean intensity, $\langle I/\sigma(I)\rangle = 5.4$ for 23652 reflections.

### Quartz crystal microbalance with dissipation

QCM-D was used to track spontaneous incorporation before the hydration step of the **HC8** into the SLB formed at the QCM silica electrode surface via fusion of SUVs of mixtures of PC (chicken egg), PS (porcine brain), and Chl. Different lipid compositions have been tried in an effort to find the SLB that had an optimal composition with a molar ratio PC/PS of 4:1, while still incorporating 20% w/w ratio of compounds and allowing an easier interpretation of the QCM and SFG experiments.

### SFG spectroscopy

Samples for SFG experiments were formed on 10-mm $CaF_2$ equilateral prisms coated with a layer of $SiO_2$ (~100 nm) (*44*). Half of the prism face was also coated with 150-nm Au for use as a reference. To form the

Downloaded from http://advances.sciencemag.org/ on May 31, 2021

bilayers, 25 μl of vesicle solution was added to 1 ml of aqueous 0.1 M PBS solution containing 0.2 M NaCl. A flow cell was formed by the $CaF_2$ prism, Teflon O-ring, and Teflon backplate with Teflon tubes as input and output ports connected to two syringes. The vesicle PBS mixture was added to one syringe and manually passed back and forth between syringes across the $CaF_2$ surface. The solution was then stationary for about 10 min to completely form the bilayer. After, excess PBS solution was used to rinse off any remaining vesicles. The laser system used for the SFG experiments was a Ti-sapphire amplifier (Coherent Legend Elite Duo) that was seeded by a Ti-sapphire oscillator (Coherent Micra-5) and provided 5 mJ, 25-fs duration, and 800-nm pulses at a repetition rate of 1 kHz (*45*). One portion of the output is spectrally narrowed with a Fabry-Perot etalon (TecOptics Inc.) to form the "visible" upconversion beam, whereas another portion is used to generate tunable broadband infrared pulses in a commercial optical parametric amplifier (Coherent OPerA Solo). The visible beam [10 μJ; 792.8 nm; FWHM (full width at half maximum), 10 $cm^{-1}$] and infrared beam (18 μJ; center frequencies of 3070, 3230, and 3670 $cm^{-1}$; FWHM, ~300 $cm^{-1}$) were focused onto the prism-liquid interface at 60° and 65°, respectively, with respect to the surface normal. The 2550- to 4000-$cm^{-1}$ frequency range was covered by setting the OPerA at three central positions. The SFG field was generated in reflection, dispersed on a diffraction grating, and imaged onto a liquid nitrogen–cooled charge-coupled device (Princeton Instruments). The polarization of the individual beams was controlled with the combination of a waveplate and polarizer. All data were normalized to the nonresonant Au signal obtained in *ppp*-polarization combination collected immediately before vertically translating the flow cell to the sample. In addition to the SFG polarization combinations shown in the main text, we also measured the interference polarization combinations (+45)pp, (−45)pp, (+45)sp, and (−45)sp, where the measured SFG polarization was set to +45° or −45°. The interference combinations mix achiral and chiral signals, measuring the norm square of $(\chi_{ppp} \pm \chi_{spp})/\sqrt{2}$ or $(\chi_{ssp} \pm \chi_{psp})/\sqrt{2}$, respectively, where $\chi$ is the second-order nonlinear susceptibility. The difference between the +45° and −45° polarization combinations is thus illustrative of a chiral response. The ±45° polarizations were measured simultaneously, providing a robust chiral detection method immune to laser fluctuations, as described by McDermott *et al.* (*38*). The interference method typically has better fidelity in detecting chirality but can be harder to interpret because of the unknown complex phase of the interference. Figure S6 shows the differences in the +45° and −45° polarizations. As expected, the interference chiral response showed clear chiral signals with a higher signal-to-noise ratio than the pure chiral measurement. The interference spectra show the same features in both the NH and OH frequency ranges, as the pure achiral and chiral responses, but are more complicated to analyze because of the interference. These data provide further proof that both the channels themselves and the channel water structures are chiral. Figure S7 shows the FTIR attenuated total reflection (ATR) spectrum of dry **HC8** powder. A band around 2800 $cm^{-1}$ due to the imidazole was observed, confirming this assignment in the SFG spectra.

## MD simulations

We performed MD simulations of artificial water channels formed by **HC8**, **R-HC8**, and **S-HC8** I-quartets following our previous protocol (*14*) that is briefly described hereafter.

### *System preparation*

On the basis of the x-ray structures, we embedded ca. 3-nm-wide I-quartet channel patches in a mixed PC/PS/Chl lipid bilayer environment. We used the Mercury 3.5.1 software to fill the crystallographic unit cell with missing molecules, and then we replicated it keeping two, six, and eight slices in *x*-, *y*-, and *z*-axis directions, respectively, resulting in a 96-molecule patch. The three **HC8**, **R-HC8**, and **S-HC8** systems include respectively two, six, and six water channels that we inserted in a pre-equilibrated triclinic membrane patch containing a 5:4:1 ratio of Chl/PC/PS molecules. We deleted overlapping water and lipid molecules and added a concentration of roughly 50 mM $Na^+Cl^-$ to the solvent, as well as an excess of $Na^+$ ions to neutralize the system charge induced by the negatively charged PS lipids.

### *MD simulation conditions*

Simulations were performed using the CHARMM-36 force field (*46*) for lipid molecules and the TIP3P model (*47*) for water. To represent the **HC8**, **R-HC8**, and **S-HC8** molecules and generate their topologies, we used the CHARMM General Force Field (*48*) together with the ParamChem web service (*49*). The GROMACS 4.6 software (*50*) was used to run the simulations with virtual interaction sites allowing a 5-fs integration time step. All bonds were constrained using the LINear Constraint Solver algorithm. Particle mesh Ewald electrostatics was used with a 10 Å cutoff with the Verlet buffer scheme for nonbonded interactions; the neighbor list was updated every 20 steps. Three baths (imidazoles, lipids, and water and ions) were coupled to a temperature of 310 K using the Bussy velocity rescaling thermostat with a time constant $\tau = 0.1$ ps. As previously determined, we chose a lateral pressure of 10 atm to maintain aggregate structuring and achieve reasonable sampling on a 500-ns time scale. Pressure in the *x*/*y* dimensions was scaled isotropically with a Berendsen weak barostat, and the *z* dimension was coupled independently to a reference pressure of 1 bar, $\tau = 5.0$ ps, and compressibility of 4.5 $10^{-5}$ $bar^{-1}$. All systems were minimized for 10000 steps with a steepest descent algorithm and equilibrated for 20 ns, using position restraints of 1000 kJ $mol^{-1}$ $nm^{-2}$ on heavy atoms, with the crystal structure as a reference. Production runs were finally computed for 500 ns without any position restraints.

## SUPPLEMENTARY MATERIALS

Supplementary material for this article is available at http://advances.sciencemag.org/cgi/content/full/4/3/eaao5603/DC1

fig. S1. Atomic displacement ellipsoid plot of the structure.
fig. S2. Incorporation of HC8 I-quartets in lipid bilayers determined by QCM-D experiments.
fig. S3. Formation of a hydration layer between an SLB and a silica substrate.
fig. S4. Surface area occupied by the single lipid molecule as a function of the hydration layer thickness.
fig. S5. Top views of water-confining I-quartet channels.
fig. S6. Difference interference SFG spectra in two polarization combinations.
fig. S7. FTIR ATR spectrum of dry HC8 powder.
fig. S8. Number of water molecules and hydrogen bonds formed by water in the membrane region.
fig. S9. Schematic representation of the O-H orientation angles that were calculated.
table S1. X-ray data collection and refinement details.
table S2. Estimate of lipid, HC8, and $H_2O$ amounts.
table S3. Estimate of the area that the single lipid molecule occupies on the available QCM-D sensor surface.
table S4. Statistics of water molecules within the lipid bilayer region.
table S5. Statistics of central channel water molecules within the lipid bilayer region.
note S1. Characterization of SLB by QCM-D.

## REFERENCES AND NOTES

1. A. Szent-Györgyi, *Cell-Associated Water* (Academic Press, 1979).
2. P. Ball, Water as an active constituent in cell biology. *Chem. Rev.* **108**, 74–108 (2008).
3. D. P. Zhong, S. K. Pal, A. H. Zewail, Biological water: A critique. *Chem. Phys. Lett.* **503**, 1–11 (2011).
4. J.-X. Cheng, S. Pautot, D. A. Weitz, X. S. Xie, Ordering of water molecules between phospholipid bilayers visualized by coherent anti-Stokes Raman scattering microscopy. *Proc. Natl. Acad. Sci. U.S.A.* **100**, 9826–9830 (2003).

Downloaded from http://advances.sciencemag.org/ on May 31, 2021

5. F. Perakis, L. D. Marco, A. Shalit, F. Tang, Z. R. Kann, T. D. Kühne, R. Torre, M. Bonn, Y. Nagata, Vibrational spectroscopy and dynamics of water. *Chem. Rev.* **116**, 7590–7607 (2016).
6. G. Hummer, A. Tokmakoff, Preface: Special topic on biological water. *J. Chem. Phys.* **141**, 22D101 (2014).
7. C. D. Ma, C. Wang, C. Acevedo-Vélez, S. H. Gellman, N. L. Abbott, Modulation of hydrophobic interactions by proximally immobilized ions. *Nature* **517**, 347–350 (2015).
8. P. Agre, Aquaporin water channels (Nobel lecture). *Angew. Chem. Int. Ed. Engl.* **43**, 4278–4290 (2004).
9. M. Barboiu, Artificial water channels. *Angew. Chem. Int. Ed.* **51**, 11674–11676 (2012).
10. M. Barboiu, Artificial water channels—Incipient innovative developments. *Chem. Commun.* **52**, 5657–5665 (2016).
11. M. Barboiu, A. Gilles, From natural to bioassisted and biomimetic artificial water channel systems. *Acc. Chem. Res.* **46**, 2814–2823 (2013).
12. Y. Le Duc, M. Michau, A. Gilles, V. Gence, Y. M. Legrand, A. van der Lee, S. Tingry, M. Barboiu, Imidazole-quartet water and proton dipolar channels. *Angew. Chem. Int. Ed. Engl.* **50**, 11366–11372 (2011).
13. E. Tajkhorshid, P. Nollert, M. Jensen, L. J. W. Miercke, J. O'Connell, R. M. Stroud, K. Schulten, Control of the selectivity of the aquaporin water channel family by global orientational tuning. *Science* **296**, 525–530 (2002).
14. E. Licsandru, I. Kocsis, Y.-x. Shen, S. Murail, Y.-M. Legrand, A. van der Lee, D. Tsai, M. Baaden, M. Kumar, M. Barboiu, Salt-excluding artificial water channels exhibiting enhanced dipolar water and proton translocation. *J. Am. Chem. Soc.* **138**, 5403–5409 (2016).
15. M. Barboiu, Supramolecular polymeric macrocyclic receptors—Hybrid carrier *versus* channel transporters in bulk liquid membranes. *J. Inclusion Phenom. Macrocyclic Chem.* **49**, 133–137 (2004).
16. A. Cazacu, Y.-M. Legrand, A. Pasc, G. Nasr, A. Van der Lee, E. Mahon, M. Barboiu, Dynamic hybrid materials for constitutional self-instructed membranes. *Proc. Natl. Acad. Sci. U.S.A.* **106**, 8117–8122 (2009).
17. A. Cazacu, C. Tong, A. van der Lee, T. M. Fyles, M. Barboiu, Columnar self-assembled ureido crown ethers: An example of ion-channel organization in lipid bilayers. *J. Am. Chem. Soc.* **128**, 9541–9548 (2006).
18. M. Michau, M. Barboiu, R. Caraballo, C. Arnal-Hérault, P. Perriat, A. van der Lee, A. Pasc, Ion-conduction pathways in self-organised ureidoarene-heteropolysiloxane hybrid membranes. *Chemistry* **14**, 1776–1783 (2008).
19. F. Hu, W. Luo, M. Hong, Mechanisms of proton conduction and gating in influenza M2 proton channels from solid-state NMR. *Science* **330**, 505–508 (2010).
20. M. Sharma, M. Yi, H. Dong, H. Qin, E. Peterson, D. D. Busath, H.-X. Zhou, T. A. Cross, Insight into the mechanism of the influenza A proton channel from a structure in a lipid bilayer. *Science* **330**, 509–512 (2010).
21. Z. F. Fei, D. Zhao, T. J. Geldbach, R. Scopelliti, P. J. Dyson, S. Antonijevic, G. Bodenhausen, A synthetic zwitterionic water channel: Characterization in the solid state by X-ray crystallography and NMR spectroscopy. *Angew. Chem. Int. Ed. Engl.* **44**, 5720–5725 (2005).
22. U. K. Eriksson, G. Fischer, R. Friemann, G. Enkavi, E. Tajkhorshid, R. Neutze, Subangstrom resolution X-ray structure details aquaporin-water interactions. *Science* **340**, 1346–1349 (2013).
23. A. S. Verkman, M. O. Anderson, M. C. Papadopoulos, Aquaporins: Important but elusive drug targets. *Nat. Rev. Drug Discov.* **13**, 259–277 (2014).
24. B. L. de Groot, H. Grubmüller, Water permeation across biological membranes: Mechanism and dynamics of aquaporin-1 and GlpF. *Science* **294**, 2353–2357 (2001).
25. N.-J. Cho, C. W. Frank, B. Kasemo, F. Höök, Quartz crystal microbalance with dissipation monitoring of supported lipid bilayers on various substrates. *Nat. Protoc.* **5**, 1096–1106 (2010).
26. E. Mahon, T. Aastrup, M. Barboiu, Dynamic glycovesicle systems for amplified QCM detection of carbohydrate-lectin multivalent biorecognition. *Chem. Commun.* **46**, 2441–2443 (2010).
27. E. Mahon, S. Garai, A. Müller, M. Barboiu, Biomimetic approach for ion channels based on surfactant encapsulated spherical porous metal-oxide capsules. *Adv. Mater.* **27**, 5165–5170 (2015).
28. G. Sauerbrey, Verwendung Von Schwingquarzen Zur Wagung Dunner Schichten Und Zur Mikrowagung. *Z. Phys.* **155**, 206–222 (1959).
29. E. Briand, M. Zäch, S. Svedhem, B. Kasemo, S. Petronis, Combined QCM-D and EIS study of supported lipid bilayer formation and interaction with pore-forming peptides. *Analyst* **135**, 343–350 (2010).
30. P. S. Cremer, S. G. Boxer, Formation and spreading of lipid bilayers on planar glass supports. *J. Phys. Chem. B* **103**, 2554–2559 (1999).
31. B. M. Auer, J. L. Skinner, Water: Hydrogen bonding and vibrational spectroscopy, in the bulk liquid and at the liquid/vapor interface. *Chem. Phys. Lett.* **470**, 13–20 (2009).
32. Y. R. Shen, *The Principles of Nonlinear Optics* (Wiley-Interscience, 1984).
33. K. B. Eisenthal, Liquid interfaces probed by second-harmonic and sum-frequency spectroscopy. *Chem. Rev.* **96**, 1343–1360 (1996).
34. L. M. Haupert, G. J. Simpson, Chirality in nonlinear optics. *Annu. Rev. Phys. Chem.* **60**, 345–365 (2009).
35. E. C. Y. Yan, L. Fu, Z. Wang, W. Liu, Biological macromolecules at interfaces probed by chiral vibrational sum frequency generation spectroscopy. *Chem. Rev.* **114**, 8471–8498 (2014).
36. E. A. Raymond, T. L. Tarbuck, M. G. Brown, G. L. Richmond, Hydrogen-bonding interactions at the vapor/water interface investigated by vibrational sum-frequency spectroscopy of HOD/$H_2O$/$D_2O$ mixtures and molecular dynamics simulations. *J. Phys. Chem. B* **107**, 546–556 (2003).
37. J. Schaefer, E. H. G. Backus, Y. Nagata, M. Bonn, Both inter- and intramolecular coupling of O–H Groups determine the vibrational response of the water/air interface. *J. Phys. Chem. Lett.* **7**, 4591–4595 (2016).
38. M. L. McDermott, H. Vanselous, S. A. Corcelli, P. B. Petersen, DNA's chiral spine of hydration. *ACS Cent. Sci.* **3**, 708–714 (2017).
39. J. Imbrogno, G. Belfort, Membrane desalination: Where are we, and what can we learn from fundamentals? *Annu. Rev. Chem. Biomol. Eng.* **7**, 29–64 (2016).
40. C. Peter, G. Hummer, Ion transport through membrane-spanning nanopores studied by molecular dynamics simulations and continuum electrostatics calculations. *Biophys. J.* **89**, 2222–2234 (2005).
41. Rigaku Oxford Diffraction, CrysAlis PRO, CrysAlis CCD and CrysAlis RED, Rigaku Oxford Diffraction, Yarnton, Oxfordshire (2015).
42. L. Palatinus, G. Chapuis, *SUPERFLIP*—A computer program for the solution of crystal structures by charge flipping in arbitrary dimensions. *J. Appl. Crystallogr.* **40**, 786–790 (2007).
43. P. W. Betteridge, J. R. Carruthers, R. I. Cooper, K. Prout, D. J. Watkin, *CRYSTALS* version 12: Software for guided crystal structure analysis. *J. Appl. Crystallogr.* **36**, 1487 (2003).
44. A. Barrett, J. Imbrogno, G. Belfort, P. B. Petersen, Phosphate ions affect the water structure at functionalized membrane surfaces. *Langmuir* **32**, 9074–9082 (2016).
45. M. L. McDermott, P. B. Petersen, Robust self-referencing method for chiral sum frequency generation spectroscopy. *J. Phys. Chem. B* **119**, 12417–12423 (2015).
46. J. B. Klauda, R. M. Venable, J. A. Freites, J. W. O'Connor, D. J. Tobias, C. Mondragon-Ramirez, I. Vorobyov, A. D. MacKerell Jr., R. W. Pastor, Update of the CHARMM all-atom additive force field for lipids: Validation on six lipid types. *J. Phys. Chem. B* **114**, 7830–7843 (2010).
47. W. L. Jorgensen, J. Chandrasekhar, J. D. Madura, R. W. Impey, M. L. Klein, Comparison of simple potential functions for simulating liquid water. *J. Phys. Chem.* **79**, 926–935 (1983).
48. K. Vanommeslaeghe, E. Hatcher, C. Acharya, S. Kundu, S. Zhong, J. Shim, E. Darian, O. Guvench, P. Lopes, I. Vorobyov, A. D. Mackerell Jr., CHARMM general force field: A force field for drug-like molecules compatible with the CHARMM all-atom additive biological force fields. *J. Comput. Chem.* **31**, 671–690 (2010).
49. K. Vanommeslaeghe, E. P. Raman, A. D. MacKerell Jr., Automation of the CHARMM General Force Field (CGenFF) II: Assignment of bonded parameters and partial atomic charges. *J. Chem. Inf. Model.* **52**, 3155–3168 (2012).
50. B. Hess, C. Kutzner, D. van der Spoel, E. Lindahl, GROMACS 4: Algorithms for highly efficient, load-balanced, and scalable molecular simulation. *J. Chem. Theory Comput.* **4**, 435–447 (2008).



**Acknowledgments**

**Funding:** This work was conducted within DYNAFUN (ANR-15-CE29-0009) (M.B.) and the LabEx CheMISyst (ANR-10-LABX-05-01) (I.K.). The study was further supported by the "Initiative d'Excellence" program from the French State (grants "DYNAMO," ANR-11-LABX-0011-01, and ANR-11-EQPX-0008). Computational work was performed using High Performance Computing (HPC) resources from GENCI-CINES (grant number 2016-072292) to M. Baaden. Funding to G.B. was from his Rensselaer Endowed Chair Fund (140124) and from the U.S. Department of Energy, Basic Energy Sciences (DE-FG02- 09ER16005) for the QCM-D measurements and calculations. H.V., S.E.S., and P.B.P. were supported by The Arnold and Mabel Beckman Foundation under a Young Investigator Award and the NSF under an NSF CAREER Award (CHE-1151079). Sample preparation made use of the Cornell Center for Materials Research Shared Facilities, which are supported through the NSF Materials Research Science and Engineering Centers program (DMR-1120296), and the Cornell NanoScale Facility, a member of the National Nanotechnology Infrastructure Network, which is supported by the NSF (ECCS-0335765). **Author contributions:** Mihail B., P.B.P., and G.B. conceived the project. I.K. and E.L. performed the synthetic work. Y.-M.L. and A.v.d.L. performed the structural analysis. I.K. and M.S. performed the QCM measurements, and H.V. and S.E.S. conducted the SFG experiments. S.M. and Marc B. performed the theoretical simulations. Mihail B. wrote the manuscript with input from all authors. **Competing interests:** The authors declare that they have no competing interests. **Data and materials availability:** All data needed to evaluate the conclusions in the paper are present in the paper and/or the Supplementary Materials. Additional data related to this paper may be requested from the authors. CCDC 1560915–1560917 contain the supplementary crystallographic data for this paper. These data can be obtained free of charge via www.ccdc.cam.ac.uk/conts/retrieving.html.

Submitted 2 August 2017
Accepted 9 February 2018
Published 23 March 2018
10.1126/sciadv.aao5603

**Citation:** I. Kocsis, M. Sorci, H. Vanselous, S. Murail, S. E. Sanders, E. Licsandru, Y.-M. Legrand, A. van der Lee, M. Baaden, P. B. Petersen, G. Belfort, M. Barboiu, Oriented chiral water wires in artificial transmembrane channels. *Sci. Adv.* **4**, eaao5603 (2018).


Downloaded from http://advances.sciencemag.org/ on May 31, 2021

Science Advances

# Oriented chiral water wires in artificial transmembrane channels

Istvan Kocsis, Mirco Sorci, Heather Vanselous, Samuel Murail, Stephanie E. Sanders, Erol Licsandru, Yves-Marie Legrand, Arie van der Lee, Marc Baaden, Poul B. Petersen, Georges Belfort and Mihail Barboiu

*Sci Adv* **4** (3), eaao5603.
DOI: 10.1126/sciadv.aao5603

**ARTICLE TOOLS** http://advances.sciencemag.org/content/4/3/eaao5603

**SUPPLEMENTARY MATERIALS** http://advances.sciencemag.org/content/suppl/2018/03/19/4.3.eaao5603.DC1

**REFERENCES** This article cites 47 articles, 7 of which you can access for free
http://advances.sciencemag.org/content/4/3/eaao5603#BIBL

**PERMISSIONS** http://www.sciencemag.org/help/reprints-and-permissions

Use of this article is subject to the Terms of Service

*Science Advances* (ISSN 2375-2548) is published by the American Association for the Advancement of Science, 1200 New York Avenue NW, Washington, DC 20005. The title *Science Advances* is a registered trademark of AAAS.

Copyright © 2018 The Authors, some rights reserved; exclusive licensee American Association for the Advancement of Science. No claim to original U.S. Government Works. Distributed under a Creative Commons Attribution NonCommercial License 4.0 (CC BY-NC).

Downloaded from http://advances.sciencemag.org/ on May 31, 2021